DOI: https://doi.org/10.15407/pmach2021.01.013

UDC 621.165+621.438

THE INFLUENCE OF MESH RESOLUTION ON 3D RANS FLOW SIMULATIONS IN TURBOMACHINERY FLOW PARTS

[1] Serhii V. Yershov
sergiy.v.yershov@gmail.com
ORCID: 0000-0002-2937-1337

[2] Viktor A. Yakovlev
yava@ipmach.kharkov.ua
ORCID: 0000-0002-6174-3022

[1] Self-employed researcher
Oulu, Finland

[2] A. Pidhornyi Institute of Mechanical Engineering Problems of NASU
2/10, Pozharskyi St.,
Kharkiv, 61046, Ukraine

The question of the difference mesh refinement degree influence on the results of calculation of the three-dimensional viscous gas flows in the flow parts of turbomachines using the RANS flow models and second order numerical methods is considered. Calculations of flows for a number of turbine and compressor grids on successively refining grids have been performed. We used H-type grids with approximate orthogonalization of cells in the boundary layer. The calculations were carried out using a CFD solver F with the use of an implicit ENO scheme of the second order, a local time step, and a simplified multigrid algorithm. When calculating the flow on fine grids, the following were used: convergence acceleration tools implemented in the solver; truncation of the computational domain with subsequent distribution of the results based on the symmetry property; the computational domain splitting into parts and computations parallelizing. Comparison of the obtained results is carried out, both in terms of qualitative resolution of the complex structure of three-dimensional flows, and in terms of quantitative assessment of losses. Grid convergence was estimated in two ways. In the first, the characteristic two-dimensional distributions of parameters obtained on different grids were visually compared. The purpose of such comparisons was to evaluate the sufficient degree of solution of both the general structure of the flow in grids and its features, namely, shock waves, contact discontinuities, separation zones, wakes, etc. The second estimation method is based on the grid convergence index (GCI). The GCI calculated from the three-dimensional density field was considered in this paper. It is concluded that for scientific research requiring high accuracy of calculations and detailing of the structure of a three-dimensional flow, very fine difference meshes with the number of cells from 10^6 to 10^8 in one blade-to-blade channel are needed, while for engineering calculations, under certain conditions, it is sufficient to use meshes with the number of cells less than 1 million in one blade-to-blade channel.

Keywords: *turbomachinery cascades, CFD, 3D RANS simulation, viscous compressible flow, grid convergence index, kinetic energy losses.*

Introduction

Currently, the computational fluid dynamics (CFD) is an essential tool for turbomachinery flows investigation and turbine and compressor flow paths designing. Nowadays, the most common approach is a numerical simulation of turbulent viscous compressible flows with the use of the Reynolds-averaged Navier-Stokes (RANS) equations. It is considered that such problem statement, as well as the used numerical methods and algorithms, are sufficiently mature, whereas corresponding CFD solvers are thoroughly tested and adjusted [1].

Nevertheless, accuracy and reproducibility of the numerical results often leave somewhat to be desired. The numerical results of the turbomachinery flow simulations may perceptibly depend on the computational mesh characteristics such as the cell shape, the size of the nearest cell to the wall y^+, the number of cells across boundary layers, the mesh expansion ratio, the curvature and non-smoothness of mesh lines, etc.

Over the past twenty years, guidelines for choosing the mesh resolution for the numerical simulation of turbomachinery viscous flows using the RANS models have changed several times: from 100-200 thousand cells per one blade-to-blade channel in 90-ies of the last century up to 0.5–1.0 million cells per blade-to-blade channel nowadays [2, 3]. Usually, a mathematical or physical basis of such recommendations is not clear, the requirements to the mesh refinement are often not well-founded [3] (perhaps, with the only exception for y^+), and in many cases the question of the solution convergence remains open.

A common practice is an approximate estimation of the grid convergence based on comparison of the following numerical results obtained using different meshes:

– some overall performance, for example efficiency (losses), forces, mass flow, etc. [4, 5];
– graphs of some parameters at solid surfaces [6, 7, 5];
– contours and numerical Schlieren images [8, 9].

In this case, one can make such comparison using some unjustified strictly quantitative estimates (for example, the difference of solutions at two different meshes is less than a certain percentage) or purely visually. The authors of the following research have quite successfully practiced all of these methods for a long time as well.

Recently, the usage of the grid convergence index (GCI), to estimate convergence, suggested by Roache [10, 11], is becoming increasingly popular. This approach consists in using a sequence of refining meshes in order to determine the apparent order of the solution convergence and the relative convergence error for some overall performance of the flow. Then, based on these data the grid convergence index is calculated, which serves as a universal criterion for comparing solution convergence using various meshes and methods of the different approximation order. It is substantiated [12] that for GCI≤1 % the solution has converged and the flow parameters at the fine mesh are slightly different from the corresponding values calculated using Richardson extrapolation. With such values of the grid convergence index, the computational results are quite suitable for studies of complex gas-dynamic phenomena. On the other hand, if GCI≤5%, then the computational results can be used for engineering purposes: to understand the general flow physics or to perform some comparative studies.

This paper, which continues the previous work of the authors [13], aims at comparing the study of the grid convergence using the grid convergence index with the traditional approximate method of the visual estimation. A special attention is paid to the analysis of both the mathematical criteria of convergence (the grid convergence index and the apparent order of the numerical method) and the quality of resolution of shock waves, tangential discontinuities, separation zones, trailing-edge wakes, etc. Based on this analysis, conclusions concerning the required mesh refinement are drawn.

Flow model and numerical techniques

We consider the 3D compressible steady statistically-averaged turbulent viscous flow through several turbomachinery stages and cascades. We use the RANS equation and the k–ω SST turbulence model [14] to describe this type of flow.

The numerical simulation was performed using our in-house CFD solver [15, 16], which is based on the implicit second-order finite-volume ENO scheme [17, 18] and a simplified multigrid algorithm that is described below. The local time step was used for the convergence acceleration. During the initial stages of the computations, the CFL number was chosen in the range from 30 to 50, and at the final stage of the computations it was reduced to 5-10 in order to improve solution accuracy. Also, during each computation the time step for excessively elongated cells was reduced according to the algorithm suggested by Frink [19].

The mathematical model, the numerical approach, the CFD solver, and comparisons with experimental data were described in detail in our previous works [15, 20, 21].

Simplified multigrid algorithm

The simplified multigrid algorithm (SMA) consists in using the set of the successively nested meshes (usually, 4 or 5 nesting levels) for each flow computation. The nested meshes are constructed in such way that increase in the current nesting level by one corresponds to the growth of the number of cells in each direction strictly by a factor of two. The flow computations begin on the coarsest of the successively nested meshes. As the convergence occurs, the numerical results are interpolated to the next finer mesh. This procedure is repeated until the solution convergence on the finest mesh is reached.

Computational meshes

We used H-type meshes with quasi-orthogonal cells in boundary layer zones near the solid walls. The meshes are refined in the boundary layer regions towards the wall as well as near the leading and trailing edges of the blades, but in the main flow they are close to uniform. The meshes considered in this study were conventionally divided into five groups based on the number of cells per one blade-to-blade channel:

1) very coarse meshes of less than 10^5 cells;
2) coarse meshes of 10^5–10^6 cells;
3) intermediate meshes of 10^6–10^7 cells;
4) fine meshes of 10^7–10^8 cells;
5) very fine meshes of more than 10^8 cells.

During the present mesh convergence study, the number of cells in each spatial direction increased by a factor of two, except for the flow case given in paragraph 9 below. For the meshes of all considered groups, value of $y+$ both in the radial and circumferential directions was set approximately equal to unity. It was found that an adequate prediction of the law of the wall (universal velocity profile) is possible only if at least 30 cells are placed across the boundary layer and the mesh expansion ratio in the wall-normal direction does not exceed 1.1.

Therefore, when we performed computations on meshes of the groups 3, 4, and 5, these requirements were strictly enforced. Ensuring these requirements on meshes of the groups 1 and 2 without reducing the accuracy in the main flow is very complicated, so in these cases trade-off decisions were taken.

Fig. 1 shows an example of a typical mesh considered in this study. To clarity, only every fourth of mesh lines is shown in each direction.

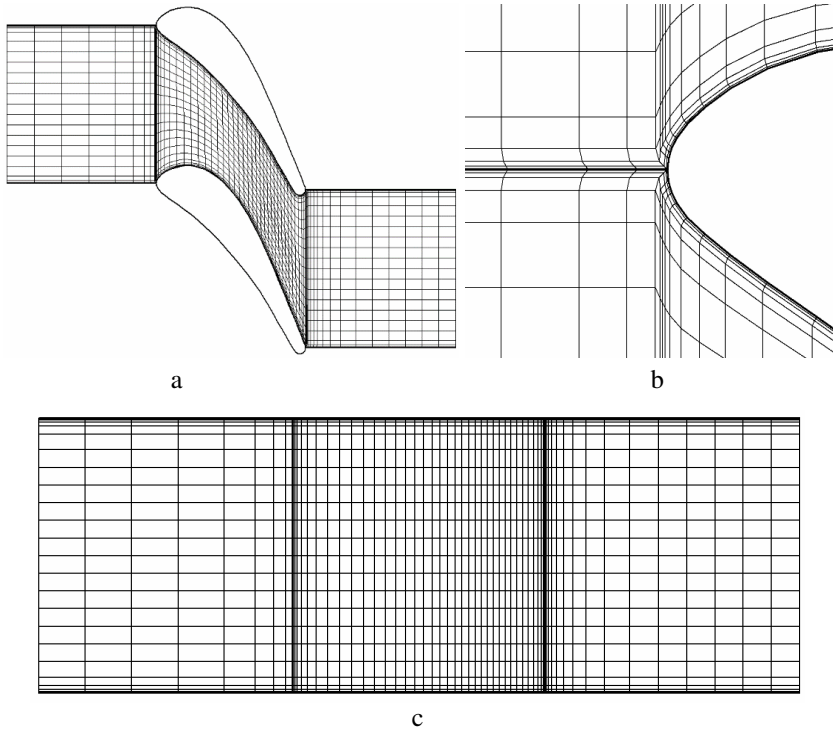

Fig. 1. The computational mesh in the VKI-Genoa turbine cascade [11]:
a – tangential section; b – mesh fragment near the leading edge;
c – meridional section

Time-marching convergence

We considered the constancy of the kinetic energy losses with a given accuracy as the main criterion of the time-marching convergence of the computations. Additionally, at the inlet and the exit of each blade row we checked the time-marching convergence of both mass flow and the turbulent kinetic energy fluxes.

It is also important to note that the convergence calculations defects made during the computations on the coarser meshes with the use of SMA, are slowly eliminated at the finer meshes, especially in small and highly elongated cells, which are generally located in the boundary layers and along the trailing-edge. Such behavior can create an illusion of the time-marching convergence of the solution. Therefore, during the computations with the use of SMA it is extremely important to ensure thoroughly the time-marching convergence of the solution at all levels of the nested meshes.

Grid convergence study technique

The main objective of this paper is to investigate the grid convergence of the numerical solution *per se* without being tied to the experimental data. It is evident that both an insufficient adequacy of the mathematical model as well as numerical and experimental errors could lead to the fact that in some cases differences between the numerical results and the experimental data may increase as the mesh is refined.

We estimated the grid convergence using two approaches. The first approach is a purely visual comparison between the characteristic two-dimensional distributions of flow parameters calculated using different meshes. Such comparisons aimed to estimate the sufficient degree of resolution of both the general pattern of cascade flows and a number of their features, namely, shock waves, tangential discontinuities, wakes, separations, etc.

The second approach for the grid convergence estimation used in this paper is based on the grid convergence index proposed by Roache [10, 11]. According to the recommendations for the grid convergence

index calculation [22], one can use the following procedure to estimate the error associated with insufficient grid convergence.

1. Three successively refined meshes are considered. These meshes are assigned indices: j=1 for the finest mesh, j=2 for the intermediate mesh, and j=3 for the coarsest mesh.

2. For each considered j-mesh, one calculates the average representative cell size h_j:

$$h_j = \left(\frac{1}{n_j} \sum_{i=1}^{n_j} \Delta V_{i,j} \right)^{1/3}, \quad (1)$$

where nj is a number of cells for the j-mesh; $\Delta V_{i,j}$ is volume of the i-cell of the j-mesh. According to the first step of the present procedure the inequality $h_1<h_2<h_3$ must hold.

3. For each pair of successively refined meshes, one calculates the grid refinement factor

$$r_{21} = h_2/h_1 \; ; \; r_{32} = h_3/h_2 \, . \quad (2)$$

4. For each of the meshes, one calculates the key variable φ_j, which will be used to estimate the grid convergence.

5. The absolute errors of the key variable are determined

$$\varepsilon_{21} = \varphi_2 - \varphi_1 \; ; \; \varepsilon_{32} = \varphi_3 - \varphi_2 \, . \quad (3)$$

6. One calculates the apparent order of the numerical method using the fixed-point iteration

$$p = \frac{1}{\ln(r_{21})} \left| \ln\left|\varepsilon_{32}/\varepsilon_{21}\right| + q(p) \right|, \quad (4)$$

where $q(p) = \ln\left(\frac{r_{21}^p - s}{r_{32}^p - s} \right)$ and $s = \operatorname{sgn}(\varepsilon_{32}/\varepsilon_{21})$.

7. One calculates the extrapolated value (using the Richardson extrapolation) of the key variable

$$\varphi_{ext} = \frac{r_{21}^p \varphi_1 - \varphi_2}{r_{21}^p - 1} \, . \quad (5)$$

8. The approximate relative error of the calculation on the finest mesh with respect to the calculation on the intermediate mesh is determined

$$e_{21} = \left| \frac{\varepsilon_{21}}{\varphi_1} \right| . \quad (6)$$

9. For the finest mesh, one calculates the grid convergence index

$$GCI_{21} = \frac{5}{4} \frac{e_{21}}{r_{21}^p - 1} \, . \quad (7)$$

The following remarks can be made on this procedure.

In the case of sufficiently fine meshes, the grid refinement factor r equals to the ratio of the mesh cell numbers and the equations 1 and 2 can be replaced as follows

$$r_{jk} = n_k/n_j \, . \quad (8)$$

The value of the grid refinement factor r according to Celik [22], should not be less than 1.3.

Equation (4) that determines the grid convergence contains two absolute value functions. One of them has the absolute error ratio as argument, and the other imposes in fact the convergence order positive if the grid refinement factor r is larger than 1. The latter does not follow from the derivation of this equation. In authors' opinion, such a misrepresentation can hide an important feature as the solution divergence, when the discretization errors increase as the mesh is refined, and the apparent grid convergence order becomes negative. Such behavior may occur not only for ill-posed problems, but also, in particular, in the case of ″numerical saturation″ of the solution, when one uses extremely fine meshes. In this study, we determine the grid convergence order as follows

$$p = \frac{1}{\ln(r_{21})}\left[\ln\left|\varepsilon_{32}/\varepsilon_{21}\right| + q(p)\right]. \quad (9)$$

It is quite obvious that the meshes to be compared should be as similar in their structure as possible, i.e., a systematic method of grid refinement is preferable to use. It is not recommended to combine meshes of different types (H-, C- and O-types). Ideally, the cells of different meshes, which are identically located in the computational domain, should be geometrically similar. This makes it possible to exclude from consideration additional errors related to different mesh structures.

This procedure works well in the case of meshes being in the asymptotic range. If the mesh is beyond it, the convergence order can significantly differ from the formal difference scheme order. This difference can occur due to rough meshes, when flow equations are not adequately approximated, or due to extremely fine meshes, if a round-off error accumulation and ″numerical saturation″ dominate over numerical errors.

In this paper, we calculate the grid convergence index for the total force f_j acting on the blades, and for the coefficient of the cascade or stage kinetic energy losses ζ_j, defined as

$$\zeta_j = \left[\frac{I_{exit} - I^{is}_{exit}}{I^{tot}_{inlet} - I^{is}_{exit}}\right]_j, \quad (10)$$

where I is the enthalpy; the superscripts *tot* and *is* represent total and isentropic parameters; the subscripts *inlet* and *exit* denote the parameters at the computational domain inlet and exit, respectively.

We calculate the isentropic enthalpy, according to the idea of Denton [23], based on the growth of entropy of perfect gas in the flow path:

$$I^{is}_{exit} = I_{exit}\left(\frac{S_{inlet}}{S_{exit}}\right)^{1/\gamma}, \quad (11)$$

where $S = p/\rho^{\gamma}$ is entropic function; p is pressure and ρ is density.

Enthalpy and entropy in equations (10) and (11) are averaged in the circumferential and radial directions.

The grid convergence index can be calculated not only for some overall performance, such as efficiency (kinetic energy losses), forces, etc., but also for 3D fields of gas-dynamic parameters. In this case, instead of values of both the key variable φ_1 in equation (6) and the absolute errors ε in equations (3), one can calculate the values of the selected flow parameter and its absolute errors, correspondingly, which are somehow averaged over the whole 3D flow field. In this paper, we consider the grid convergence index calculated on the base of the 3D density field.

Usually, the relative errors and the grid convergence index are written in percentage terms, which is done in this paper.

Subsonic flow within the VKI-Genoa cascade

We considered a subsonic flow in the VKI-Genoa turbine cascade that has been experimentally investigated by Ubaldi [24], and Cicatelli and Sieverding [25]. This is a straight cascade with the exit Mach number M_{1is}=0.24. We performed the computations using the meshes of about 8 thousand cells, 65 thousand cells, 520 thousand cells, and 4.2 million cells.

Fig. 2 shows the Mach number contours at the midspan section in the cases of the meshes of 520 thousand cells (Fig. 2, a) and 4.2 million cells (Fig. 2, b). It is clearly seen that the solutions are quite similar.

Table 1 shows the grid convergence study for the VKI-Genoa cascade. The grid convergence of the kinetic energy losses, the total force acting on the blade, and the 3D density field in the blade-to-blade channels are investigated in this and further cases. Subscripts ζ, f and ρ correspond to the grid convergence parameters calculated for the kinetic energy losses, the total force and the 3D density field, respectively. Here and below, the grid convergence index for j-mesh is calculated using the computational results for j-mesh and two coarser meshes, $j-1$ and $j-2$.

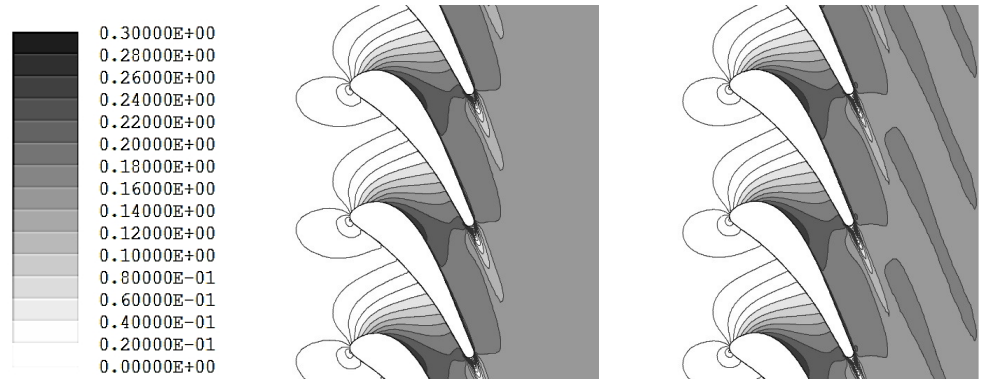

Fig. 2. The Mach number contours at the midspan section of the VKI-Genoa turbine cascade: a – mesh of 5.2·105 cells; b – mesh of 4.2·106 cells

Table 1. Grid convergence for the VKI-Genoa turbine cascade

Number of cells	Mesh group	ζ	ζ_{ext}	p_ζ	$e_{21,\zeta}$	GCI_ζ	f [N]	f_{ext} [N]	p_f	$e_{21,f}$	GCI_f	p_ρ	GCI_ρ
$8.2\cdot10^3$	1	0.317	–	–	–	–	162.1	–	–	–	–	–	–
$6.5\cdot10^4$		0.188	–	–	–	–	168.0	–	–	–	–	–	–
$5.2\cdot10^5$	2	0.127	0.072	1.08	48.00	53.90	170.0	171.1	1.55	1.19	0.78	2.04	0.07
$4.2\cdot10^6$	3	0.123	0.123	4.00	3.08	0.26	171.0	171.8	1.09	0.56	0.62	1.26	0.84

An analysis of the numerical results shows that different parameters have different grid convergence rates. The solution convergence order p varies from 1 to 2, except for the case of ″superconvergence″ in the kinetic energy losses for the finest mesh of the group 3. Also note the excessively high kinetic energy losses in the case of the coarse mesh of the group 1. These two anomalies are not observed for the grid convergence of other considered parameters. It allows us to assume that the asymptotic convergence range for kinetic energy losses is somewhat narrower than for other parameters, and, in this case, the meshes of the groups 1 and 3 are out of it. In this flow case the mesh of the group 3 with about 4.2 million cells is characterized by the grid convergence index less than unity for all the considered parameters. This mesh is turn to be sufficient for modeling the flow in the present turbine cascade.

Based on the above results, the authors have chosen the computational mesh for the further investigation of the fully turbulent and transitional flow in this cascade [20, 21].

Transonic flow through the ABB-Saturn turbine stage

We considered the numerical simulation of flow within the turbine stage of the company ABB-Saturn [26]. In this flow case both cascades are annular, the flow through them is transonic and the exit flow conditions were M_{1is}=0.87 for the stator cascade and M_{w2is}=0.71 for the rotor cascade. The computations were performed using the meshes of about 4 thousand cells, 30 thousand cells, 240 thousand cells, 1.9 million cells, and 15.3 million cells per each blade-to-blade channel of the stator and rotor cascades.

Fig. 3 and 4 show the numerical flow patterns at the midspan section of the stator and rotor cascades, respectively for computations using the meshes of the groups 2-4. The numerical Schlieren images are given for the different meshes, whereas the Mach number contours are presented only for the finest mesh.

It is clearly seen from the figures that in the case of the meshes of the group 2 (Fig. 3, a and 4, a) the shock waves are blurred and it is difficult to define their position precisely. In the case of the mesh of the 3rd group (Fig. 3, b and 4, b), the shocks are captured better. A clear shock wave pattern is obtained only using the mesh of the group 4 (Fig. 3, c and 4, c). Using this mesh, we detected a small separation zone in the rotor cascade that slightly changes the shock wave configuration. The separation in the stator cascade and the trailing-edge wakes downstream of both cascades are also best resolved on the finest mesh.

It should be noted that here and further the numerical Schlieren images contain computational artefacts in the form of horizontal (axial) and vertical (circumferential or radial) lines near the leading and trailing edges. This phenomenon takes place in the areas of the significant mesh refinement and indicates the loss of accuracy, which manifests itself in a large error in determination of the flow parameters derivatives.

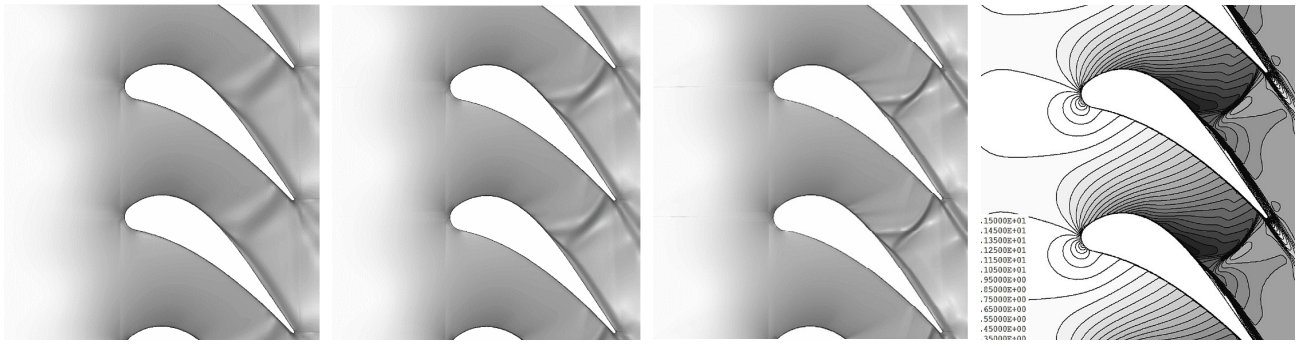

a b c d

Fig. 3. The flow pattern at the midspan section of the stator cascade of the ABB-Saturn turbine stage:
a, b, c – numerical Schlieren (meshes of $2.4 \cdot 10^5$, $1.9 \cdot 10^6$ and $1.5 \cdot 10^7$ cells, respectively);
d – Mach number contours (mesh of $1.5 \cdot 10^7$ cells)

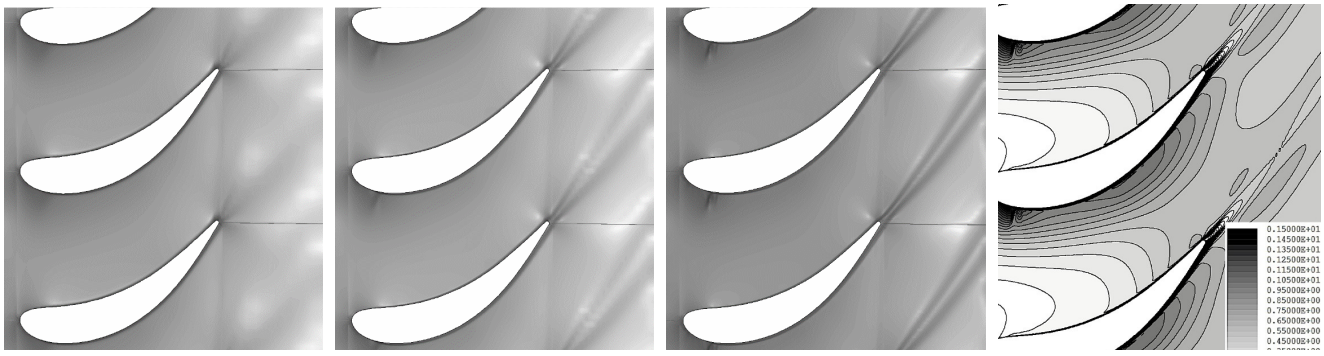

a b c d

Fig. 4. The flow pattern at the midspan section of the rotor cascade of the ABB-Saturn turbine stage:
a, b, c – numerical Schlieren (meshes of $2.4 \cdot 10^5$, $1.9 \cdot 10^6$ and $1.5 \cdot 10^7$ cells, respectively);
d – Mach number contours (mesh of $1.5 \cdot 10^7$ cells)

Fig. 5 demonstrates the numerical Schlieren images at the cross-flow sections downstream of the stator (Fig. 5, a, b, c) and rotor (Fig. 5, d, e, f) cascades at the distance of about 10 percent of the blade axial chord in the cases of computations with the use of the meshes of the 2nd group (Fig. 5, a, d), the group 3 (Fig. 5, b, e), and the 4th group (Fig. 5, c, f). Each image shows three blade-to-blade channels of the annular cascade. It can be seen that in the case of meshes of the group 2, the trailing-edge wakes are fuzzy, especially downstream of the stator cascade, and the secondary flows in the endwall zones are quite indistinguishable. The resolution of trailing-edge wakes and secondary flows improves considerably in the case of meshes of the group 3, and is the clearest in the case of meshes of the 4th group.

Table 2 shows the grid convergence study in the case of the turbine stage flow computations. We considered the turbine stage kinetic energy losses, the total force acting on the rotor blades, and the 3D density field in the turbine stage as key variables. There is a tendency of the solution convergence when the mesh is refined. The grid convergence order of different parameters on different meshes ranges from 0.9 to 1.5, with the exception of the case of the total force acting on the rotor blades for the mesh of the group 2. In the last case, there is a solution divergence (negative apparent convergence order) on coarse meshes. In the case of the fine mesh of the group 4, which contains about 30 million cells within the turbine stage flow path, the grid convergence index for both the total force and the 3D density field is less than 1. At the same time, the values of the grid convergence index and the relative error calculated using the kinetic energy losses on this mesh, are quite large and are about 8 and 5 percent, respectively. This fact agrees with the mentioned above differences in the fields of the gas-dynamic parameters on the meshes of the groups 3 and 4 and shows that the meshes of 15 million cells per a blade-to-blade channel may be insufficient for the assured grid convergence in the case of a turbine stage flow. Nevertheless, such degree of convergence can be quite sufficient for high-volume engineering computations.

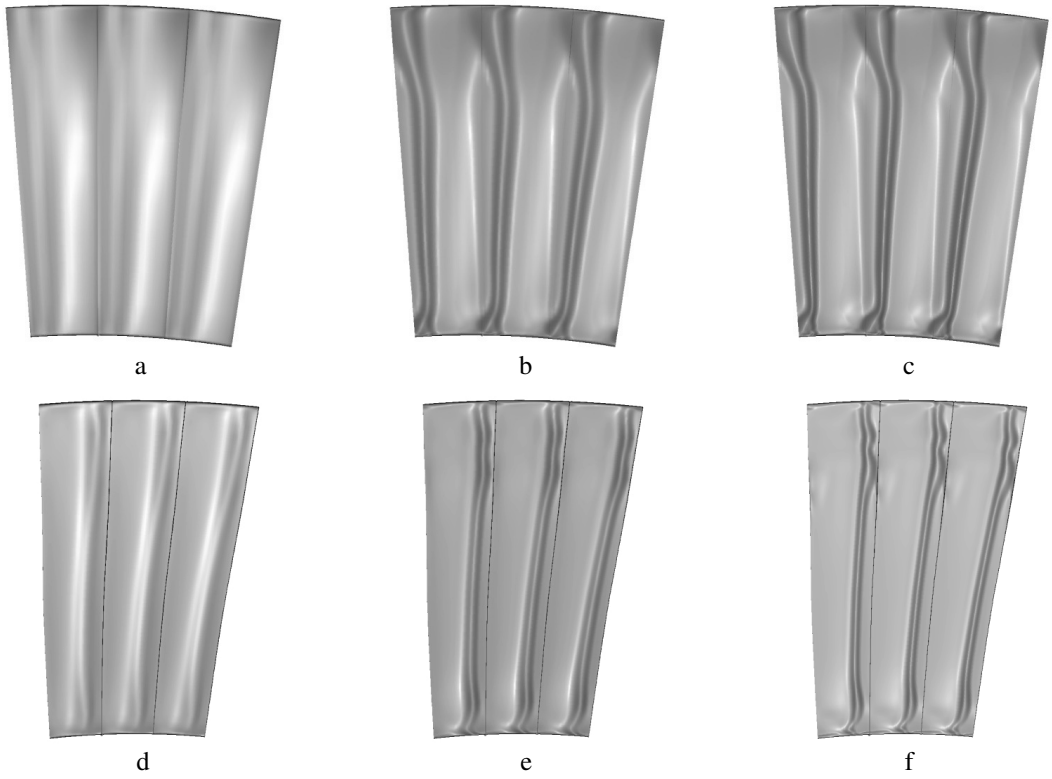

Fig. 5. The numerical Schlieren images at the crosswise sections of the ABB-Saturn turbine stage:
a, b, c – downstream of the stator trailing edges (meshes of $2.4 \cdot 10^5$, $1.9 \cdot 10^6$ and $1.5 \cdot 10^7$ cells, respectively); d, e, f – downstream of the rotor trailing edges (meshes of $2.4 \cdot 10^5$, $1.9 \cdot 10^6$ and $1.5 \cdot 10^7$ cells, respectively)

Table 2. Grid convergence for the ABB-Saturn turbine stage

Number of cells	Mesh group	ζ	ζ_{ext}	p_ζ	$e_{21,\zeta}$	GCI_ζ	f [N]	f_{ext} [N]	p_f	$e_{21,f}$	GCI_f	p_ρ	GCI_ρ
$2 \times 3.8 \cdot 10^3$	1	0.177	–	–	–	–	205.2	–	–	–	–	–	–
$2 \times 3.0 \cdot 10^4$		0.129	–	–	–	–	214.0	–	–	–	–	–	–
$2 \times 2.4 \cdot 10^5$	2	0.112	0.103	1.50	15.20	10.40	226.1	259.3	-0.45	5.33	-25.0	0.225	16.10
$2 \times 1.9 \cdot 10^6$	3	0.103	0.093	0.92	8.74	12.30	230.9	234.0	1.33	2.07	1.71	0.925	1.61
$2 \times 1.5 \cdot 10^7$	4	0.098	0.092	0.85	5.10	7.97	232.5	233.4	1.52	0.72	0.48	1.148	0.54

Supersonic flow within the compressor cascade of the EU FP7 research project TFAST

We considered supersonic flow through the straight compressor cascade, which has been experimentally and computationally studied in the EU FP7 program project, TFAST [27]. According to the experimental conditions, the boundary layer was extracted at the endwalls to reduce corner separations and secondary flows. The computations were carried out at the compression ratio π_k=1.22 with the relative inlet Mach number M_{1w}=1.2 using the meshes of about 0.8 million cells, 2.4 million cells, 9.2 million cells, 54 million cells, and 250 million cells. All these meshes, excluding the coarsest and the finest ones, at the tangential section were the same as the 2D meshes used in [28]. In this computational case, the grid refinement factor r varied for different meshes from 1.46 to 1.8.

Fig. 6 demonstrates the numerical Schlieren images of the flow pattern at the midspan section for the different meshes. It is seen that in the case of the meshes of the group 3 (Fig. 6, a and 6, b) all shock waves are blurred. In the case of the mesh of the group 4 (Fig. 6, c) the resolution of the bow shock is improved, but the reflection of the leading-edge oblique shock impinging on the blade suction side as well as the non-smeared shock wave pattern near cascade throat and downstream are clearly captured only in the case of the mesh of the group 5 (Fig. 6, d). The mesh refinement significantly improves the flow separation and trailing-edge wake resolution, especially capturing the tangential discontinuities downstream of the triple-shock points. In the case of the mesh of the group 5 the resolution of the main flow features is the best, compared to other considered meshes.

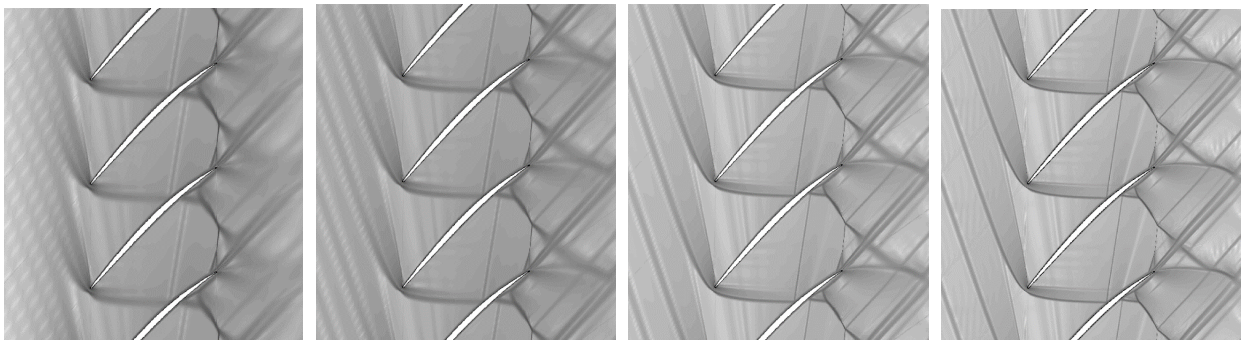

a b c d

Fig. 6. The numerical Schlieren images at the midspan section of the TFAST compressor cascade: a, b, c, d – meshes of $2.4 \cdot 10^6$, $9.2 \cdot 10^6$, $5.4 \cdot 10^7$, $2.5 \cdot 10^8$ cells, respectively

Table 3 shows the grid convergence study in the case of the compressor cascade flow computations. The grid convergence order on the mesh of the 3rd group varies from 1.1 to 1.9. The meshes of the groups 4 and 5 appear to be out of the asymptotic convergence range when the kinetic energy losses are a key variable, since ″superconvergence″ is observed. Owing to this fact, in the case of the finest mesh one can observe the convergence of the calculated kinetic energy losses to their extrapolated value. The grid convergence indices in the cases of meshes of the 4th and 5th groups are less than 1 percent. In the case of the finest mesh of the group 5, the grid convergence order of the total force is negative, which apparently indicates "numerical saturation" of the solution and means that the total force calculated with the use of this mesh is beyond the asymptotic convergence range.

Table 3. Grid convergence for the TFAST compressor cascade for π_c = 1.22 conditions

Number of cells	Mesh group	ζ	ζ_{ext}	p_ζ	$e_{21,\zeta}$	GCI_ζ	f [N]	f_{ext} [N]	p_f	$e_{21,f}$	GCI_f	p_ρ	GCI_ρ
$7.7 \cdot 10^5$	2	0.1727	–	–	–	–	260.2	–	–	–	–	–	–
$2.4 \cdot 10^6$	3	0.1496	–	–	–	–	266.9	–	–	–	–	–	–
$9.2 \cdot 10^6$		0.1373	0.1284	1.94	8.96	8.07	269.7	271.7	1.94	1.00	0.94	1.056	7.371
$5.4 \cdot 10^7$	4	0.1342	0.1337	3.31	2.31	0.48	271.5	273.2	1.30	0.68	0.77	0.923	0.416
$2.5 \cdot 10^8$	5	0.1340	0.1340	4.59	0.15	0.02	273.3	290.5	-0.18	0.67	-9.68	0.440	0.763

Transonic flow within the turbine cascade of the EU FP7 research project TFAST

We considered transonic flow in the turbine cascade, which has been computationally and experimentally studied in the EU FP7 program project, TFAST [27]. This is a straight cascade with the exit Mach number M_{1is}=1.05. We calculated the cascade flow using the meshes of about 11 thousand cells, 85 thousand cells, 680 thousand cells, 5.4 million cells, and 43.5 million cells. Film cooling simulation was provided using air blowing through two rows of holes uniformly spaced along the blade (46 holes in each row). The area of each hole was about 0.5 mm^2, whereas the blade length and chord were 125 mm and 76 mm, respectively. We did not consider the cascade flow with film cooling using the meshes of the group 1, since in this case the wall-surface area of near-wall cells was much larger than the cooling hole area. In the case of the meshes of the groups 3 and 4 we used from 1 to 4 cells per one hole and from 6 to 16 cells per one hole, respectively.

Fig. 7 presents the Mach number contours at the midspan section of the blade-to-blade channel for different meshes. In the case of film cooling, the image patches near the leading edges are shown. These figures demonstrate that the mesh refinement significantly improves the resolution of the shock waves and trailing-edge wakes. So, in the case of the meshes of the groups 2 (Fig. 7, a) and 3 (Fig. 7, b) the resolution of the first shock wave at the suction side just downstream of the cascade throat is unsatisfactory, and only in the case of the mesh of the group 4 (Fig. 7, c) this shock wave can be definitely interpreted as a discontinuity.
The cooling gas jets are also better resolved on the finer meshes. It is clearly seen from Fig. 7 that in the case of the mesh of the group 3 (Fig. 7, d) the cooling jets cling to the blade suction side, whereas in the case of the mesh of the group 4 (Fig. 7, e) they penetrate much further into the main flow.

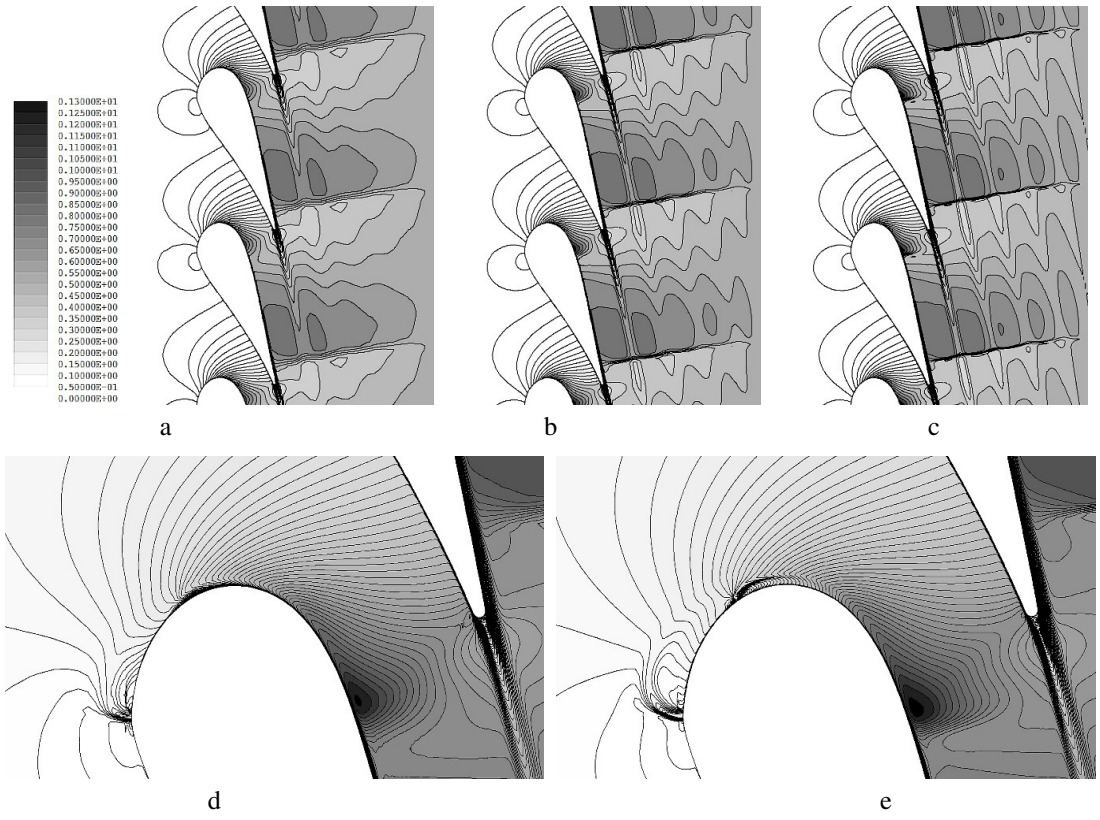

Fig. 7. The Mach number contours at the midspan section of the TFAST turbine cascade:
a, b, c – without film cooling (meshes of $6.8 \cdot 10^5$, $5.4 \cdot 10^6$ and $4.35 \cdot 10^7$ cells, respectively);
d, e – with film cooling (meshes of $5.4 \cdot 10^6$ and $4.35 \cdot 10^7$ cells, respectively)

Table 4 shows the grid convergence study in the case where we don't consider film cooling. There is a tendency of the solution convergence, while the mesh is refined. The grid convergence order varies from 0.3 to 2.1 for various parameters and meshes. The grid convergence index is less than 1 in the case of the mesh of the group 4 for all considered parameters, and it is greater than 1 only for kinetic energy losses in the case of the mesh of the group 3.

Table 4. Grid convergence for the TFAST turbine cascade without film cooling

Number of cells	Mesh group	ζ	ζ_{ext}	p_ζ	$e_{21,\zeta}$	GCI_ζ	f [N]	f_{ext} [N]	p_f	$e_{21,f}$	GCI_f	p_ρ	GCI_ρ
$1.1 \cdot 10^4$	1	0.0916	–	–	–	–	491.4	–	–	–	–	–	–
$8.5 \cdot 10^4$		0.0653	–	–	–	–	492.6	–	–	–	–	–	–
$6.8 \cdot 10^5$	2	0.0575	0.0542	1.75	13.60	7.15	492.4	492.4	2.75	0.04	0.01	0.998	1.29
$5.4 \cdot 10^6$	3	0.0524	0.0428	0.61	9.73	22.90	492.2	493.2	0.39	0.05	0.20	1.123	0.50
$4.3 \cdot 10^7$	4	0.0512	0.0508	2.09	2.34	0.90	492.0	491.0	0.28	0.04	0.24	0.590	0.31

The results of a similar study of the grid convergence for this flow case with film cooling are given in Table 5. The grid convergence order varies from 0.9 to 1.4, and the grid convergence index in the case of the mesh of the group 4 for all parameters is less than 1%, except for the kinetic energy losses, for which it is slightly less than 2 percent. Despite the low values of both the grid convergence index and the relative error, the authors doubt that in this case the solution has converged. These doubts are confirmed by the abovementioned comparisons in Fig. 7, d, e, where it is seen that the numerical solution continues to change even on the finest mesh: the cooling gas jets penetrate much deeper into the main flow when the mesh is refined. The increase in the kinetic energy losses on the mesh of the group 4 is explained by the increased perturbation of both the boundary layer and the flow core due to cooling jets. The effect of the cooling jets on the cascade losses seems to be of the same order of magnitude as the error of a double mesh refinement, therefore, the value of the grid convergence index does not reflect the convergence process.

Table 5. Grid convergence for the TFAST turbine cascade with film cooling

Number of cells	Mesh group	ζ	ζ_{ext}	p_ζ	$e_{21,\zeta}$	GCI_ζ	f [N]	f_{ext} [N]	p_f	$e_{21,f}$	GCI_f	p_ρ	GCI_ρ
$6.8\cdot10^5$	2	0.0589	–	–	–	–	492.6	–	–	–	–	–	–
$5.4\cdot10^6$	3	0.0567	–	–	–	–	491.9	–	–	–	–	–	–
$4.3\cdot10^7$	4	0.0577	0.0585	1.14	1.73	1.81	491.7	491.5	1.44	0.05	0.04	0.904	0.40

Computational time

Table 6 gives the computational time of all considered flow cases and some additional data related therewith. The data on the computational time per one time step and number of time steps are given for the finest mesh of each considered flow case (the highest nesting level of SMA). We rounded the number of time steps and the computational time.

Table 6. Computational time

Cascade (stage)	Number of cells	Dimensions	Number of mesh levels	Memory, GB	Time per one time step, s	Number of time steps	Time, days
VKI-Genoa	$4.19\cdot10^6$	128×128×256	4	0.75	15	60000	12
ABB-Saturn	$3.07\cdot10^7$	2×194×208×384	5	2×2.8=5.6	59	80000	60
TFAST turbine	$4.35\cdot10^7$	368×224×528	5	9.5	157	100000	195
TFAST compressor	$2.48\cdot10^8$	496×496×1008	5	3×16.4=49.2	121	200000	370

Also, some comments concerning the special conditions of the computational experiments are presented below.

The parallelization of the computations of flow through the ABB-Saturn turbine stage was carried out using the standard tools of our in-house solver (one blade row per one CPU core/thread). Contrariwise, we performed the computations of flow within the TFAST compressor cascade (which has the straight blade and flat plate endwalls) using the truncated computational domain of one half of the blade span and the symmetry conditions at the cutting plane. When parallelizing the computations in this flow case, the computational domain was divided into three blocks in the axial direction. Since the communication between the blocks was time-consuming, the data exchanges were carried out once in the specified number of time steps. The ENO derivatives and the viscous terms also were "frozen" during several time steps to accelerate the calculations. These features are not implemented yet in the standard version of the code F, but will be included in the future.

We have performed the turbomachinery flow computations using the following PCs operating under OS Windows 7:

– Intel Core i7-4820, 3.7 GHz, RAM 64 GB (the meshes of the groups 4 and 5);

– Intel Core i7-3770, 3.5 GHz, RAM 32 GB and 16 GB (the meshes of the groups 1–4).

Conclusions

This study confirms the well-known fact that the mesh scales should match the flow scales, namely the characteristic size of the flow regions with significant gradients of thermodynamic, kinematic and turbulent parameters. These requirements dictate the use of sufficiently fine meshes of at least an order of 10^7 cells per one blade-to-blade channel when using the second order-accurate numerical scheme in the case of the RANS computations. A good resolution of shock waves, flow separation zones, trailing-edge wakes, and tangential discontinuities needs such meshes. An additional mesh refinement may be necessary due to various small-scale features of flow or flow path geometry, such as film cooling holes, vortex generators, etc.

The study of grid convergence using the grid convergence index allows us to make the following remarks. As well as during time-marching iterations, the kinetic energy losses showed the slowest convergence compared with the total force and the three-dimensional density field. In addition, we have found that the kinetic energy losses have a narrower range of the asymptotic convergence than that of other considered parameters. Apparently, viscous and inviscid parameters have different convergence behavior, and, therefore, it is preferable to use the grid refinement factor less than 2 and closer to 1.3-1.5.

If the grid refinement study is based on convergence of the kinetic energy losses and the mesh of the group 1 is used as the coarsest mesh, then the grid convergence index may increase when the mesh is refined. This is due to the fact that estimation of the kinetic energy losses with the use of very coarse meshes may be

inadequate. We observed such a phenomenon for the mesh of 3rd group in the cases of both the ABB-Saturn turbine stage (see Table 2) and the TFAST turbine cascade (see Table 4) and it confirms a narrow range of asymptotic convergence for the kinetic energy losses.

If fine meshes are used and ″numerical saturation″ is observed, then the apparent order of the grid convergence can be either quite high, indicating ″superconvergence″, or even negative. In the former case the grid convergence index is usually small enough, but in the latter case it is negative and, likely, high in magnitude. In this study, the numerical solution obtained for the TFAST compressor flow case using the finest mesh of the 5th group with 250 million cells in the blade-to-blade channel (Table 3) is as an example of such behavior. On the other hand, the numerical solution can demonstrate tangible changes when the mesh is refined, while the grid convergence index for some parameters turns to be small enough. In the following research, examples of this discrepancy are numerical simulations of the flow through the ABB-Saturn stage using the mesh of the group 4 with about 15 million cells per each blade-to-blade channel (Table 2) and especially the flow case of the TFAST turbine cascade with film cooling (Table 5). All this allows us to conclude that estimation of the grid convergence index by itself is not sufficient for a conclusive analysis of the grid convergence. An examination of the magnitude and sign of the apparent convergence order, the magnitude of the relative error, and also the comparison of the solutions obtained using different meshes visually can provide additional important information regarding grid convergence.

Concerning the recommendations for the choice of the mesh refinement, we can conclude the following. Scientific studies of the fine flow patterns that aim at very high accuracy and a detailed resolution require extremely fine meshes, so, in this case, preference should be given to the meshes of the groups 4 and 5. However, such computations are known to be very time-consuming and ″time vs. resolution″ trade-off decision is permissible. Therefore, it can be acceptable to use intermediate meshes of the group 3. Of course, the mentioned above requirements on the near-wall cell size, on the number of cells across a boundary layer, and on the mesh expansion ratio in the wall-normal direction should be strictly satisfied in this case. In the case of high-volume industrial computations, aimed at either improving or comparing turbomachinery flow paths, the use of intermediate (of the group 3) or even coarser meshes may be sufficient. However, one should keep in mind that such computations often result in the increased flow path efficiency by only 0.001–0.002 (0.1–0.2 percentage points), which is comparable with discretization errors or even less ones. Therefore, the final results of such computations should always be verified with the use of finer meshes.

References

1. Hirsch, C. (2007). Numerical computation of internal and external flows: The fundamentals of computational fluid dynamics. Elsevier, Butterworth-Heinemann, 680 p. https://doi.org/10.1016/B978-0-7506-6594-0.X5037-1.
2. ERCOFTAC: Official website, 2020. URL: https://www.ercoftac.org.
3. CFD Online: Official website, 2020. URL: https://www.cfd-online.com.
4. Rautaheimo, P., Salminen, E., & Siikonen, T. (2003). Numerical simulation of the flow in the NASA low-speed centrifugal compressor. *International Journal of Turbo and Jet Engines*, vol. 20, iss. 2, pp. 155–170. https://doi.org/10.1515/TJJ.2003.20.2.155.
5. Diskin, B., Thomas, J., Rumsey, C. L., & Schwoeppe, A. (2015). Grid convergence for turbulent flows (Invited). *Proceeding of the 53rd AIAA Aerospace Sciences Meeting,* Kissimmee, Florida, USA, AIAA Paper 2015-1746, 50 p. https://doi.org/10.2514/6.2015–1746.
6. Gerolymos, G. A., Tsanga, G., & Vallet, I. (1998). Near-wall k-e computation of transonic turbomachinery flows with tip clearance. *AIAA Journal*, vol. 36, no. 10, pp. 1769–1777. https://doi.org/10.2514/2.275.
7. Duchaine, F., Maheu, N., Moureau, V., Balarac, G., & Moreau, S. (2014). Large-eddy simulation and conjugate heat transfer around a low-mach turbine blade. *Journal of Turbomachinery*, vol. 136, iss. 5, pp. 051015-051025. https://doi.org/10.1115/1.4025165.
8. Prikhodko, A. A. & Polevoy, O. B. (2004). *K raschetu prostranstvennykh turbulentnykh otryvnykh techeniy* [On the calculation of spatial turbulent separated flows]. *Aerogidrodinamika: problemy i perspektivy – Aerohydrodynamics: problems and prospects*. Kharkov: National Aerospace University ″Kharkiv Aviation Institute″, pp. 73–87 (in Russian).
9. Su, X., Yamamoto, S., & Yuan, X. (2013). On the accurate prediction of tip vortex: Effect of numerical schemes. *Proc. of the ASME Turbo Expo 2013: Turbine Technical Conference and Exposition,* San Antonio, TX, USA, ASME Paper GT2013-94660, 15 p. https://doi.org/10.1115/GT2013-94660.
10. Roache, P. J. (1994). Perspective: A method for uniform reporting of grid refinement studies. *Journal of Fluids Engineering*, vol. 116, iss. 3, pp. 405–413. https://doi.org/10.1115/1.2910291.

11. Roache, P. J. (1997). Quantification of uncertainty in computational fluid dynamics. *Annual Review of Fluid Mechanics*, vol. 29, pp. 123–160. https://doi.org/10.1146/annurev.fluid.29.1.123.
12. Hemez, F. M. & Tippetts, T. B. (2007). Successes and failures of verifying the convergence of discrete solutions. *IMAC-XXV: Proceedings of the Conference & Exposition on Structural Dynamics*, Orlando, Florida, USA, pp. 1686–1698.
13. Yershov, S. V. & Yakovlev, V. A. (2015). *O vybore stepeni izmelcheniya setki pri raschetakh trekhmernykh techeniy vyazkogo gaza v turbomashinakh* [On the choice of the degree of mesh refinement when calculating three-dimensional viscous gas flows in turbomachines]. *Vestnik dvigatelestroyeniya – Herald of Aeroengine-building*, no. 2, pp. 171–177 (in Russian).
14. Menter, F. R. (1994). Two-equation eddy-viscosity turbulence models for engineering applications. *AIAA Journal*, vol. 32, no. 8, pp. 1598–1605. https://doi.org/10.2514/3.12149.
15. Yershov, S., Yakovlev, V., Derevyanko, A., Gryzun, M., & Kozyrets, D. (2012). The development of new CFD solver for 3D turbomachinery flow computations. *Cieplne Maszyny Przepływowe. Turbomachinery*, Politechnika Łódzka, Łódź, Poland, no. 141, pp. 15–24.
16. Yershov, S. V. (2012). *Razvitiye kompleksa programm dlya rascheta trekhmernykh techeniy vyazkogo gaza* [Development of a software package for calculating three-dimensional viscous gas flows]. *Aviatsionno-kosmicheskaya tekhnika i tekhnologiya – Aerospace Technic and Technology,* no. 5(92), pp. 89–94 (in Russian).
17. Yershov, S. V. (1994). *Kvazimonotonnaya ENO skhema povyshennoy tochnosti dlya integrirovaniya uravneniy Eylera i Navye–Stoksa* [Quasimonotone ENO scheme of increased accuracy for integrating the Euler and Navier – Stokes equations]. *Matematicheskoye modelirovaniye – Mathematical Models and Computer Simulations*, vol. 6, no. 11, pp. 63–75 (in Russian).
18. Grizun, M. N. & Yershov, S. V. (2013). *Chislennoye modelirovaniye mnogomernykh szhimayemykh techeniy s pomoshchyu metoda Nyutona* [Numerical modeling of multidimensional compressible flows using Newton's method]. *Vestnik NTU «KHPI». Seriya: Energeticheskiye i teplotekhnicheskiye protsessy i oborudovaniye – Bulletin of the NTU "KhPI". Series: Power and Heat Engineering Processes and Equipment*, no. 13, pp. 38–46 (in Russian).
19. Frink, N. T. (1996). Assessment of an unstructured-grid method for predicting 3-D turbulent viscous flows. *Proceedings of the AIAA 34th Aerospace Sciences Meeting and Exhibit*, Reno, NV, USA, AIAA Paper 96-0292, 12 p. https://doi.org/10.2514/6.1996-292.
20. Yershov, S., Derevyanko, A., Yakovlev, V., & Gryzun, M. (2016). Influence of laminar-turbulent transition on 3D flow pattern in subsonic turbine cascade. *Proceedings of the 2016 Propulsion and Energy Forum. 52nd AIAA/SAE/ASEE Joint Propulsion Conference*, Salt-Lake-City, UT, USA, AIAA Paper 2016-4552, 17 p. https://doi.org/10.2514/6.2016-4552.
21. Yershov, S. & Yakovlev, V. (2016). Validation of the PTM transition model on a 3D flow through a turbine cascade. in *IMECE 2016: Proceedings of the ASME 2016 International Mechanical Engineering Congress and Exposition*, Phoenix, AZ, USA, IMECE, 2016-65001, 11 p. https://doi.org/10.1115/IMECE2016-65001.
22. Celik, I. B., Ghia, U., Roache, P. J., Freitas, C. J., Coleman, H., & Raad, P. E. (2008). Procedure for estimation and reporting of uncertainty due to discretization in CFD applications. *Journal of Fluids Engineering (Special Publication)*, vol. 130, no 7, pp. 078001-1–078001-4. https://doi.org/10.1115/1.2960953.
23. Denton, J. (1993). Loss mechanisms in turbomachines. *Journal of Turbomachinery*, vol. 115, iss. 4, pp. 621–656. https://doi.org/10.1115/1.2929299.
24. Ubaldi, M., Zunino, P., Campora, U., & Ghiglione, A. (1996). Detailed velocity and turbulence measurements of the profile boundary layer in a large scale turbine cascade. *Proceedings of the International Gas Turbine and Aeroengine Congress and Exhibition*, Birmingham, UK, ASME 96-GT-42, 14 p. https://doi.org/10.1115/96-GT-042.
25. Cicatelli, G. & Sieverding, C. H. (1997). The effect of vortex shedding on the unsteady pressure distribution around the trailing edge of a turbine blade. *Journal of Turbomachinery*, vol. 119, no. 4, pp. 810–819. https://doi.org/10.1115/1.2841192.
26. Granovskiy, A. V. (2011). *Razrabotka metodov povysheniya gazodinamicheskoy effektivnosti vysokonagruzhennykh stupeney okhlazhdayemykh gazovykh turbin* [Development of methods for increasing the gas-dynamic efficiency of highly loaded stages of cooled gas turbines]: Thesis for the doctor of science degree in engineering. Moscow: Moscow Power Engineering Institute (in Russian).
27. Transition Location Effect on Shock Wave Boundary Layer Interaction: Official website, 2020. URL: http://tfast.eu.
28. Papazov, S. V., Yakovlev, V. A., & Yershov, S. V. (2014). *Chislennoye modelirovaniye techeniya v kompressornoy reshetke v shirokom diapazone rezhimov obtekaniya* [Numerical simulation of a flow in a compressor lattice in a wide range of flow regimes]. *Problemy mashinostroyeniya – Journal of Mechanical Engineering,* vol. 17, no. 4, pp. 3–9 (in Russian).

Received 23 February 2021

Вплив сіткового розділення на 3D RANS моделювання течій у проточних частинах турбомашин

[1] С. В. Єршов, [2] В. А. Яковлєв

[1] Самозайнятий дослідник, Оулу, Фінляндія

[2] Інститут проблем машинобудування ім. А. М. Підгорного НАН України,
61046, Україна, м. Харків, вул. Пожарського, 2/10

Розглядається вплив ступеня подрібнення різницевої сітки на результати розрахунку тривимірних течій в'язкого газу в проточних частинах турбомашин при використанні моделей течії RANS і чисельних методів другого порядку. Виконано розрахунки течій для ряду турбінних та компресорних решіток на послідовно подрібнюваних сітках. Використовувалися сітки типу H з наближеною ортогоналізацією комірок в примежовому шарі. Розрахунки проводилися за допомогою CFD розв'язувача F з використанням неявної ENO схеми другого порядку, локального кроку за часом і спрощеного багатосіткового алгоритму. При розрахунку течії на дрібних сітках застосовувалися: засоби прискорення збіжності, реалізовані в розв'язувачі; усічення розрахункової області з подальшим поширенням результатів на основі властивості симетрії; розбиття розрахункової області на частини і розпаралелювання обчислень. Проведено зіставлення отриманих результатів як за якісним розділенням складної структури тривимірних потоків, так і за кількісною оцінкою втрат. Сіткова збіжність оцінювалася двома способами. У першому візуально порівнювалися характерні двовимірні розподіли параметрів, отримані на різних сітках. Метою таких порівнянь було оцінити достатній ступінь розв'язку як загальної структури течії в решітках, так і її особливостей, а саме, стрибків ущільнення, контактних розривів, відривних зон, слідів та ін. Другий спосіб оцінки ґрунтується на індексі сіткової збіжності (GCI). GCI може бути визначений не тільки для інтегральних характеристик течії, таких, як втрати, сили і т. д., але і для тривимірних полів газодинамічних параметрів, зокрема розглядався GCI, розрахований за тривимірним полем щільності. Зроблено висновок, що для наукових досліджень, які вимагають високої точності розрахунків і деталізації структури тривимірної течії, потрібні дуже дрібні різницеві сітки, з кількістю комірок від 10^6 до 10^8 в одному міжлопатковому каналі, в той час як для інженерних розрахунків, при виконанні деяких умов, досить сіток з кількістю комірок менше 1 млн в одному міжлопатковому каналі.

Ключові слова: *решітки турбомашин, CFD, 3D RANS моделювання, в'язка стискальна течія, індекс сіткової збіжності, втрати кінетичної енергії.*

Література

1. Hirsch C. Numerical computation of internal and external flows: The fundamentals of computational fluid dynamics. Elsevier, Butterworth-Heinemann, 2007. 680 p. https://doi.org/10.1016/B978-0-7506-6594-0.X5037-1.
2. ERCOFTAC: офіційний веб-сайт, 2020. URL: https://www.ercoftac.org.
3. CFD Online: офіційний веб-сайт, 2020. URL: https://www.cfd-online.com.
4. Rautaheimo P., Salminen E., Siikonen T. Numerical simulation of the flow in the NASA low-speed centrifugal compressor. *Intern. J. Turbo and Jet Engines.* 2003. Vol. 20. Iss. 2. P. 155–170. https://doi.org/10.1515/TJJ.2003.20.2.155.
5. Diskin B., Thomas J., Rumsey C. L., Schwoeppe A. Grid convergence for turbulent flows (Invited). *Proceeding of the 53rd AIAA Aerospace Sci. Meeting*, Kissimmee, Florida, USA. AIAA. 2015. Paper 2015-1746. 50 p. https://doi.org/10.2514/6.2015–1746.
6. Gerolymos G. A., Tsanga G., Vallet I. Near-wall k-e computation of transonic turbomachinery flows with tip clearance. *AIAA J*. 1998. Vol. 36. No. 10. P. 1769–1777. https://doi.org/10.2514/2.275.
7. Duchaine F., Maheu N., Moureau V., Balarac G., Moreau S. Large-eddy simulation and conjugate heat transfer around a low-mach turbine blade. *J. Turbomachinery*. 2014. Vol. 136. Iss. 5. P. 051015-051025. https://doi.org/10.1115/1.4025165.
8. Приходько А. А., Полевой О. Б. К расчету пространственных турбулентных отрывных течений. *Аэрогидродинамика: проблемы и перспективы*. Харьков: Нац. аэрокосм. ун-т «Харьк. авиац. ин-т». 2004. С. 73–87.
9. Su X., Yamamoto S., Yuan X. On the accurate prediction of tip vortex: Effect of numerical schemes. *Proc. ASME Turbo Expo 2013: Turbine Tech. Conf. and Exposition,* San Antonio, TX, USA. ASME. 2013. Paper GT2013-94660. 15 p. https://doi.org/10.1115/GT2013-94660.
10. Roache P. J. Perspective: A method for uniform reporting of grid refinement studies. *J. Fluids Eng*. 1994. Vol. 116. Iss. 3. P. 405–413. https://doi.org/10.1115/1.2910291.
11. Roache P. J. Quantification of uncertainty in computational fluid dynamics. *Annual Review Fluid Mech*. 1997. Vol. 29. P. 123–160. https://doi.org/10.1146/annurev.fluid.29.1.123.

12. Hemez F. M., Tippetts T. B. Successes and failures of verifying the convergence of discrete solutions. *IMAC-XXV: Proc. Conf. & Exposition on Structural Dynamics*, Orlando, Florida, USA, 2007. P. 1686–1698.
13. Ершов С. В., Яковлев В. А. О выборе степени измельчения сетки при расчетах трехмерных течений вязкого газа в турбомашинах. *Вестн. двигателестроения*. 2015. № 2. С. 171–177.
14. Menter F. R. Two-equation eddy-viscosity turbulence models for engineering applications. *AIAA J*. 1994. Vol. 32. No. 8. P. 1598–1605. https://doi.org/10.2514/3.12149.
15. Yershov S., Yakovlev V., Derevyanko A., Gryzun M., Kozyrets D. (2012). The development of new CFD solver for 3D turbomachinery flow computations. *Cieplne Maszyny Przepływowe. Turbomachinery*. Politechnika Łódzka, Łódź, Poland. No. 141. P. 15–24.
16. Ершов С. В. Развитие комплекса программ для расчета трехмерных течений вязкого газа. *Авиац.-косм. техника и технология.* 2012. № 5 (92). С. 89–94.
17. Ершов С. В. Квазимонотонная ENO схема повышенной точности для интегрирования уравнений Эйлера и Навье-Стокса. *Мат. моделирование*. 1994. Т. 6. № 11. С. 63–75.
18. Гризун М. Н., Ершов С. В. Численное моделирование многомерных сжимаемых течений с помощью метода Ньютона. *Вест. НТУ «ХПИ», Сер.: Энергетические и теплотехнические процессы и оборудование.* 2013. № 13. С. 38–46.
19. Frink N. T. Assessment of an unstructured-grid method for predicting 3-D turbulent viscous flows. *Proc. AIAA 34th Aerospace Sci. Meeting and Exhibit*, Reno, NV, USA. AIAA. 1996. Paper 96-0292. 12 p. https://doi.org/10.2514/6.1996-292.
20. Yershov S., Derevyanko A., Yakovlev V., Gryzun M. Influence of laminar-turbulent transition on 3D flow pattern in subsonic turbine cascade. *Proc. 2016 Propulsion and Energy Forum. 52nd AIAA/SAE/ASEE Joint Propulsion Conf.*, Salt-Lake-City, UT, USA, AIAA. 2016. Paper 2016-4552. 17 p. https://doi.org/10.2514/6.2016-4552.
21. Yershov S., Yakovlev V. Validation of the PTM transition model on a 3D flow through a turbine cascade. in *IMECE 2016: Proc. ASME 2016 Intern. Mech. Eng. Congress and Exposition*, Phoenix, AZ, USA, 2016. IMECE 2016-65001. 11 p. https://doi.org/10.1115/IMECE2016-65001.
22. Celik I. B., Ghia U., Roache P. J., Freitas C. J., Coleman H., Raad P. E. Procedure for estimation and reporting of uncertainty due to discretization in CFD applications. *J. Fluids Eng. (Special Publication)*. 2008. Vol. 130. No 7. P. 078001-1–078001-4. https://doi.org/10.1115/1.2960953.
23. Denton J. Loss mechanisms in turbomachines. *J. Turbomachinery*. 1993. Vol. 115. Iss. 4. P. 621–656. https://doi.org/10.1115/1.2929299.
24. Ubaldi M., Zunino P., Campora U., Ghiglione A. Detailed velocity and turbulence measurements of the profile boundary layer in a large scale turbine cascade. *Proc. Intern. Gas Turbine and Aeroengine Congress and Exhibition*, Birmingham, UK. ASME. 1996. 96-GT-42. 14 p. https://doi.org/10.1115/96-GT-042.
25. Cicatelli G., Sieverding C. H. The effect of vortex shedding on the unsteady pressure distribution around the trailing edge of a turbine blade. *J. Turbomachinery*. 1997. Vol. 119. No. 4. P. 810–819. https://doi.org/10.1115/1.2841192.
26. Грановский А. В. Разработка методов повышения газодинамической эффек-тивности высоконагруженных ступеней охлаждаемых газовых турбин: дис. … д-ра техн. наук: 05.04.12 / Моск. энерг. ин-т. М. 2011. 217 с.
27. Transition Location Effect on Shock Wave Boundary Layer Interaction: офіційний веб-сайт, 2020. URL: http://tfast.eu.
28. Папазов С. В., Яковлев В. А., Ершов С. В. Численное моделирование течения в компрессорной решетке в широком диапазоне режимов обтекания. *Пробл. машиностроения*. 2014. Т. 17. № 4. С. 3–9.